TISSUE ENGINEERING: Part A
Volume 00, Number 00, 2024

DOI: 10.1089/ten.tea.2023.0279

termis
Tissue Engineering
& Regenerative Medicine
International Society

Open camera or QR reader and scan code to access this article and other resources online.

ORIGINAL ARTICLE

Posttranscriptional Modification to Modulate Progenitor Differentiation on Heterotypic Spheroids

Nazmiye Celik, PhD,[1,2] Srinivas V. Koduru, PhD,[3] Dino J. Ravnic, DO,[4] Ibrahim T. Ozbolat, PhD,[1,2,5–8] and Daniel J. Hayes, PhD[2,5,6]

Cell aggregates are widely used to study heterotypic cellular interactions during the development of vascularization *in vitro*. In this study, we examined heterotypic cellular spheroids made of adipose-derived stem cells and $CD34^{+}/CD31^{-}$ endothelial progenitor cells induced by the transfection of miR-148b mimic for *de novo* induction of osteogenic differentiation and miR-210 mimic for *de novo* induction of endotheliogenesis, respectively. The effect of the microRNA (miRs) mimic treatment group and induction time on codifferentiation was assessed in spheroids formed of transfected cells over the course of a 4-week culture. Based on gene and protein markers of osteogenic and endotheliogenic differentiation, as well as mineralization assays, our results showed that miRs directed cell differentiation and that progenitor maturity influenced the development of heterotypic cellular regions in aggregates. Overall, the success of coculture to create a prevascularized bone model is dependent on a number of factors, particularly the induction time of differentiation before combining the multiple cell types in aggregates. The approach that has been proposed could be valuable in creating vascularized bone tissue by employing spheroids as the building blocks of more complex issues through the use of cutting-edge methods such as 3D bioprinting.

Keywords: miRNA, progenitors, osteogenesis, endotheliogenesis, paracrine signaling, spheroids, vascularization, bone

Impact Statement

Biofabrication of heterotypic adipose-derived cell aggregates using miRs has implications for those aiming to drive simultaneous differentiation of osteogenic and endotheliogenic components for 3D complex bone tissue generation. The findings shown here suggest that the cross-talk between miR-induced progenitors is affected by the relative maturity of these osteogenic and endotheliogenic progenitors.

[1]Engineering Science and Mechanics Department, The Pennsylvania State University, University Park, Pennsylvania, USA.
[2]The Huck Institutes of the Life Sciences, The Pennsylvania State University, University Park, Pennsylvania, USA.
[3]Gene Arrays, Omelette Inc., New York, New York, USA.
[4]Department of Surgery, The Pennsylvania State Health Milton S. Hershey Medical Center, Hershey, Pennsylvania, USA.
[5]Biomedical Engineering Department, The Pennsylvania State University, University Park, Pennsylvania, USA.
[6]Materials Research Institute, The Pennsylvania State University, University Park, Pennsylvania, USA.
[7]Neurosurgery Department, The Pennsylvania State College of Medicine, Hershey, Pennsylvania, USA.
[8]Medical Oncology Department, Cukurova University, Adana, Turkey.

Introduction

During the past two decades, bone tissue engineering techniques have become one of the most promising alternative approaches for the treatment of critical-sized bone defects.[1–3] Three-dimensional (3D) scaffold-free constructs, such as cell aggregates, have received much attention as they more accurately mimic the features of complex native tissue microenvironment. Two-dimensional (2D) culture techniques have some notable limitations including a limited expansion area, loss of cells' clonal and differentiation potential following long-term cell passaging, and a lack of dynamic microenvironment that is similar to the native tissue microenvironment, which play key roles in the regulation of stem cell differentiation.[4] In contrast to 2D, 3D culture methods are better able to recapitulate the native tissue microenvironment and facilitate complex tissue formation using multiple cell types. However, to realize this potential in tissue engineering, a major hurdle must be overcome in the development of sufficient vascular networks to deliver nutrients, oxygen, and cytokines to maintain viability in large-scale tissue grafts.[2,3,5] As such, vascularization is arguably the most important practical limitation in the use of cell aggregates toward scalable biofabrication tissues.

A form of mesenchymal stem cell which has been isolated from adipose tissue and called adipose-derived stem cells (ADSCs) has generated much interest for potential use in bone tissue regeneration. The use of these cells *in vivo* in segmental defects has shown that they can promote osteogenesis and endotheliogenesis by secreting potent growth factors such as bone morphogenic protein (BMP), vascular endothelial growth factor (VEGF), and fibroblast growth factor-2 .[6–8] ADSCs have additionally been shown to be capable of endothelial differentiation and tube formation in coculture systems.[7,9] Moreover, CD34 is an essential marker to identify vascular endothelial progenitor cells (EPCs)[10] and CD31 is widely regarded as a marker for mature endothelial cells (ECs).[11] Our previous study showed that $CD34^+/CD31^-$ cells isolated from the adipose stromal vascular fraction (SVF) showed VEGF-induced EC phenotype *in vitro*.[12] However, there are still difficulties to be overcome in forming stable vascular structures capable of integrating with endogenous vasculature *in vivo*.

Coculturing ECs or EPCs with osteoprogenitors has been explored for promotion of vascularized tissue formation.[13,14] Tissue engineering has used coculture systems that include mature ECs and ADSCs to discover the functions of angiogenic factors required to create mature and stable vascular network growth.[15–18] Several studies have also used coculture system of ADSCs for osteogenic tissue formation with mature ECs, such as human umbilical vein endothelial cells (HUVECs).[19–21] Although HUVECs enhance osteogenesis when cocultured with ADSCs *in vitro*, using of mature differentiated cells such as HUVECs often results in poor tissue integration, reduced tissue volume, and can result in a robust host response.[22–24] Studies have also showed that while the rate of differentiation of stem cells to osteoblasts was affected by the presence of mature ECs, mature osteoblasts or stem cells did not affect the rate of differentiation of EPCs.[25] In addition, regardless of the cell maturation rates, each cell type has specific nutrient requirements and requires a corresponding specific medium composition. When multiple distinct cell types are cocultured, they can have very different media requirements to promote cell-type specific proliferation and differentiation.

There is a need to have a better understanding of the molecular mechanisms that modulate the codevelopment of osteogenic and endotheliogenic differentiation in parallel from human stem cells. This codifferentiation process may be achieved through transient genetic modification of ADSCs using microRNAs (miRs). To the best of our knowledge, no study has focused on the interactions between paracrine factors and miRs specifically in ADSC differentiation.[26] It is particularly important because up to 30% of human genes may be controlled by miRs, according to bioinformatics studies.[27] MiR expression has tissue or cell specificity,[28] where they can act as key regulators in diverse biological processes, such as early development, cell proliferation, differentiation, migration and apoptosis, depending on the expression of the miR targets.[29] MiRs have the ability to regulate a number of signaling pathways and transcription factors involved in osteoblast differentiation.[26] Several miRNAs have been found that modulate osteogenic differentiation in ADSCs, including miR-148b.[24,30] Previous studies have showed that miR-148b induces osteogenic differentiation *de novo* in bone marrow-derived stem cells (BMSCs) and ADSCs by upregulating BMPs and inducing alkaline phosphatase (ALP) activity.[24,31–33] Studies have also revealed that miR-210, known as the master hypoximiR,[34] could induce endothelial differentiation and angiogenesis.[24,35–37] In this process, miRs may be necessary for the commitment and differentiation of ADSCs into specific lineages.[37,38] Studies have showed that the expression of paracrine signals are modulated by miRs.[39] Collectively, better understanding of the interactions between paracrine signals and miRs, and of their effect on the development of vascularized osteogenic tissues, will help advance new strategies to improve treatment of segmental bone defects caused by diseases, such as osteonecrosis,[40] osteomylitis,[41] and osteoporosis.[42]

In this study, we evaluated the impact of codifferentiation of endothelial and osteogenic progenitor cells induced by miRs on the development of early vascularization in heterotypic cellular bone spheroids. In particular, we examined the codifferentiation with miR-148b-transfected ADSCs and miR-210-transfected $CD34^+/CD31^-$ cells combined at different induction time points toward osteogenic and endotheliogenic lineages, respectively. We performed mineralization and biochemical essays, as well as gene and protein level assessments of osteogenic and endotheliogenic differentiation markers.

Materials and Methods

Human ADSCs and $CD34^+/CD31^-$ Cell Isolation and Culture

With the patients' consent and approval, conducted under the Institutional Review Board protocol (IRB protocol #4972), surgically discarded adipose tissues were obtained from patients, undergoing elective panniculectomy at Pennsylvania State University (Hershey, PA). Human ADSCs and $CD34^+/CD31^-$ cells were isolated from these tissues. The tissue samples were chopped and washed with Hanks balanced salt solution (HBSS) several times to eliminate any remaining blood.[12,24] Minced adipose tissue was digested with 0.2% of collagenase (Gibco,

Gaithersburg, MD) and incubated at 37°C on a shaker for 2 h. The collagenase-digested tissue was centrifuged for 10 min at 2,000 rpm and the pellet was obtained. After resuspending the pellet in red blood cell lysis buffer, large tissue particles were removed by serial filtration through 40 μm and 100 μm filters followed by centrifugation. The SVF was obtained by resuspending the pellet in HBSS buffer and separating it on a Ficoll gradient centrifuge for 30 min at 2,000 rpm. This produced the white layer band. For human ADSCs, the SVF was resuspended in magnetic activated cell sorting (MACS) buffer and passed through an AutoMACs Pro cell sorter (Milteyni Biotec, CA) to separate ADSCs using CD90 microbeads. Flow cytometry was performed to confirm the results with stem cell-specific markers CD73 and CD90[12]. To isolate human $CD34^+/CD31^-$ cells, we first used Miltenyi Biotec, CA, microbeads to remove $CD31^-$ cells from SVF. After the depletion of CD31, the cells were sorted using autoMACS Pro (Miltenyi Biotec, CA) and tagged with $CD34^+$ microbeads. Flow cytometry was used to assess the purity of isolated $CD34^+$ cells. Briefly, BD Cytofix (BD Biosciences PharMingen, Franklin Lakes, NJ) was used to fix $CD34^+$ cells after they were centrifuged to produce a cell pellet.[12] The cells were then washed and resuspended in BD perm wash buffer for 10 min. CD34 cells were then resuspended in perm/wash buffer with primary antibody, CD34-FITC, CD31-PE (BD Biosciences, Franklin Lakes, NJ), and incubated at room temperature for 30 min and washed. Labeled cells were acquired by a LSR-II flow cytometer (BD Biosciences, Franklin Lakes, NJ) and the data were analyzed using FlowJo (Ashland, OR) software.[12] Human ADSCs and $CD34^+/CD31^-$ cells that were previously sorted were cultured at 37°C with 5% CO_2 in Dulbecco's modified Eagle medium (DMEM)/F12 supplement containing 20% fetal bovine serum (FBS), 100 U/mL penicillin, and 100 μg/mL streptomycin. Every 3 days, the cell medium was replaced.

Osteogenic and Endotheliogenic Differentiation with Chemical Transfection via miRs

DMEM/F12, lipofectamine RNAiMAX transfection reagent, and Opti-Minimum Essential Medium (MEM)-reduced serum medium were purchased from ThermoFisher Scientific (Waltham, MA). Custom oligonucleotides (miR-148b: 5′-UCAGUGCAUCACAGAACUUUGU-3′; miR-210: 5′-CUGUGCGUGUGACAGCGGCUGA-3′) were ordered from Integrated DNA Technologies (Coralville, IA).[24] Cells were seeded in 175 cm^3 cell culture flasks at a density of 1×10^6. ADSCs were transfected by miR-148b and human $CD34^+/CD31^-$ cells were transfected by miR-210 mimic separately when cells reached a confluence of 80% before being seeded in opti-MEM medium (Gibco, Carlsbad, CA) for 24 h. Invitrogen Lipofectamine RNAiMAX transfection reagent was used for transfection and mixed with miR-148b or -210 according to the manufacturer's protocol. The transfection process took over 24 h. The final concentration of miR-148b and -210 in opti-MEM medium was determined to be 200 nM per 175 cm^3 cell-culture flasks. The final concentration of miR-148b and miR-210 in the opti-MEM medium was 200 nM for a volume of 10 mL based on results from our previous studies.[24,43] The miRNA mimic solution in opti-MEM at a concentration of 200 nM was transferred to 175 cm^2 cell-culture flasks and incubated at 37°C and 5% CO_2 for 24 h. Trypsinization was used to collect transfected cells for the use in making of spheroids.

Transfection Efficiency

Custom fluorescence-labeled oligonucleotides (miR-210: 5′ 6-Cy5-CUG UGC GUG UGA CAG CGG CUG A- 3′; miR-148b: 5′ UCA GUG CAU CAC AGA ACU UUG U 6-FAM 3′) were sourced from Integrated DNA Technologies (Coralville, IA). Cells were seeded at an initial density of 2×10^5 in 75 cm^2 cell-culture flasks. The ADSCs and $CD34^+/CD31^-$ cells were transfected, in separate flasks, by Fluorescein amidite (FAM)-labeled miR-148b and Cy5-labeled miR-210 mimic, respectively. The transfected cells were collected by trypsination to determine the transfection efficiency via flow cytometry (BD Bioscience, USA). Three groups, unlabeled (nontransfected) $CD34^+/CD31^-$ cells, a 1:4 ($CD34^+/CD31^-$ cells: ADSCs) ratio of transfected cells, and Cy5-labeled (transfected) $CD34^+/CD31^-$ cells, were created for analysis. Approximately, 1×10^5 cells were collected for each flow cytometry analysis by Phosphate Buffered Saline (PBS) with 0.2% FBS (Supplementary Figs. S2–S3).

Osteogenic Induction by Differentiation Medium

Basal media HyClone DMEM/F12 (Hyclone, Marlborough, MA) was supplemented with 10% FBS and 1% antibiotic solution (10,000 μg mL^{-1} penicillin and streptomycin). For the osteogenic differentiation as a positive control group, basal media was supplemented with ascorbate-2-phosphate (50 μM), dexamethasone (0.1 μM), and β-glycerophosphate (10 mM) used for the culture of spheroids at 37°C and 5% CO_2. We changed the medium every 3 days.

Fabrication of Spheroids

To fabricate spheroids, both human ADSCs and $CD34^+/CD31^-$ cells were harvested with trypsin and collected by centrifugation at 1,600 rpm for 5 min. Cells were reconstituted to 2.5×10^5 cells per mL consisting of a mixed population of 80% ADSCs and 20% $CD34^+/CD31^-$ cells in basal medium. The cell suspension (200 mL) was pipetted into a single well of a U-bottom 96-well microplate (Greiner Bio-One, Monroe, NC). The plates were then placed in the incubator for the formation of spheroid overnight at 37°C in a humid atmosphere with 5% CO_2. The basal medium used to grow spheroids was changed every 3 days. The osteogenic media was used to differentiate spheroids osteogenically as the positive control group, and the medium was changed every 3 days. The fabricated spheroids were removed from the U-bottom wells by forcefully pipetting the growth media up and down after 28 days of differentiation (Fig. 1).

We evaluated three different stages in our experiments. We called the stages as the initial stage if the induction time was 2 days for the miR-148b transfection, the early stage if the induction time was 6 days for the miR-148b transfection, and the middle stage if the induction time was 12 days for the miR-148b transfection. Each of the stages are also evaluated as changing the induction time of miR-210 transfection as 2 days, 6 days, and 12 days. The reader is referred to Table 1 for the groups' information. In addition to Table 1, we evaluated spheroids formed with only $CD34^+/CD31^-$ cells after 2 days transfection by miR-210, spheroids composed of $CD34^+/CD31^-$

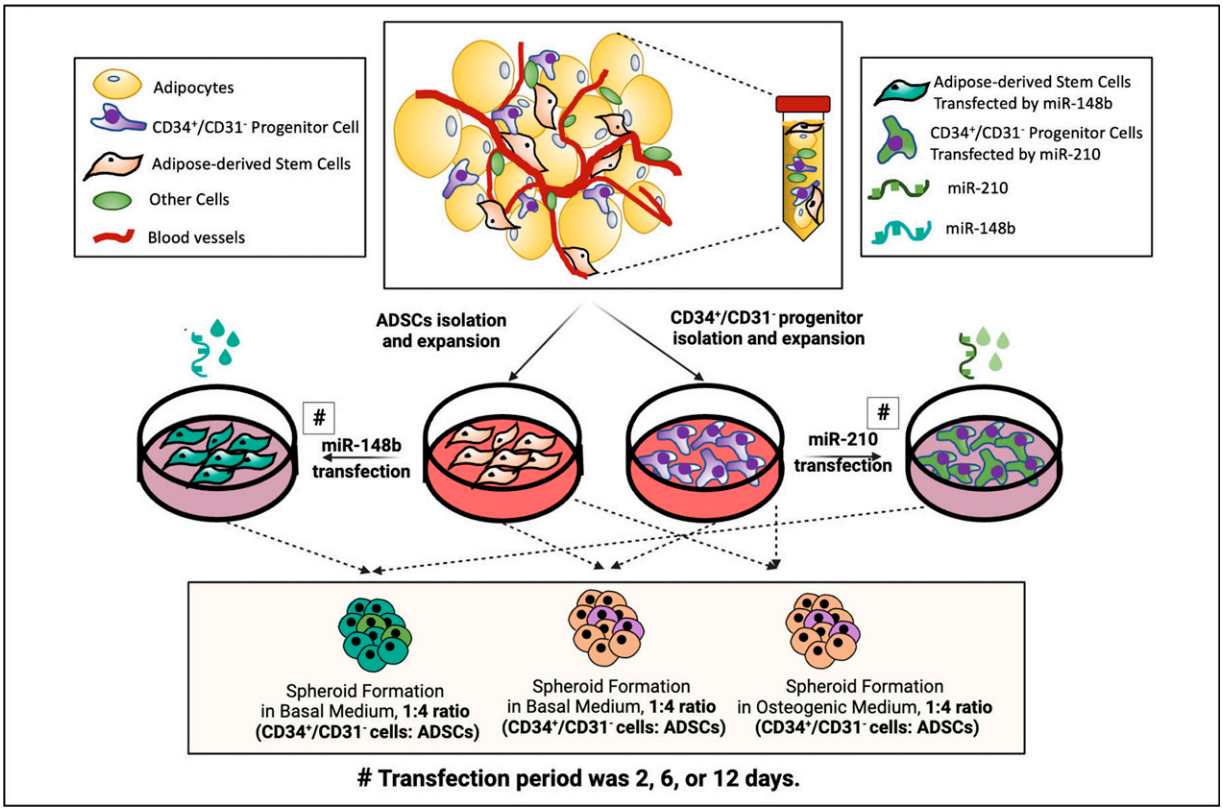

FIG. 1. The schematic diagram of the process to fabricate spheroids made of cells transfected by miR-210 and -148 b.

cells after 12 days transfection by miR-210, and spheroids composed of nontransfected (control) $CD34^+/CD31^-$ cells for preliminary studies (Supplementary Fig. S1).

Gene Expression Using Quantitative Real-Time Polymerase Chain Reaction

To evaluate the osteogenic and endotheliogenic gene expression profiles using quantitative real-time polymerase chain reaction (qRT-PCR), three different groups for initial, early, and late stages were harvested at days 14 and 28. Samples were homogenized in TRIzol reagent (Life Technologies, Carlsbad, CA) and PureLink RNA Mini Kit (Thermo Fisher Scientific, Waltham, MA) according to the manufacturer's protocol. A Nanodrop (Thermo Fisher Scientific, PA) was used to measure the concentration of RNA. Reverse transcription was performed using AccuPower® CycleScript RT PreMix (BIONEER, Daejeon, Korea) following the manufacturer's instructions. Gene expression was analyzed quantitatively with SYBR Green (Thermo Fisher Scientific, Pittsburg, PA) using a QuantStudio 3 PCR system (Thermo Fisher Scientific, Waltham, MA). Osteogenic and endotheliogenic genes evaluated included angiopoietin-1 (ANGPT-1), collagen type-1 (Col-1), platelet/EC adhesion molecule-1 (PECAM-1), runt-related transcription factor-2 (RUNX2), osteocalcin (OCN), BMP-4, bone sialoprotein (BSP), and ALP. Refer to Table 2 for the gene sequences. Expression levels for each gene were then normalized to glyceraldehyde 3-phosphate dehydrogenase (GAPDH). The fold change of ADSC spheroids after formation at Day 2 was set as one-fold and values in osteogenic groups were normalized with respect to that of the group.[43,44]

Mineralization staining

Histological analysis was used to evaluate the hydroxyapatite deposition of spheroids for each group and stage following 14 and 28 days of culture. Spheroids were first washed with Dulbecco's Phosphate Buffered Saline (DPBS) and then left overnight at room temperature (25°C) in 10% neutral buffered formalin. Samples were gradually dehydrated in alcohol and embedded in paraffin using a Leica TP 1020 automatic tissue processor (Leica, Buffalo Grove, IL). Then, samples were sectioned in 10-mm thickness. To evaluate mineralization, the Osteoimage™ Mineralization Assay (Lonza) was used. After three room temperature washes with Osteoimage™ wash buffer, sectioned spheroids were incubated for 30 min in the dark at room temperature with 2 mL of staining reagent.[24]

Immunofluorescence Staining and Histochemistry

Spheroids that had been cultured for 28 days were fixed in 10% formalin for 60 min after being rinsed three times with DPBS for each group. Samples were processed through an automated tissue processor (Leica TP 1020) and gradually dehydrated in alcohol before being embedded in paraffin. Samples were then divided into 10-mm-thick sections. Samples that had been sectioned were permeabilized for 10 min in 0.2% Triton X-100, and then blocked for 60 min at room temperature using 2.5% normal goat serum (NGS).[24] Samples were incubated with antirunx2 primary antibody (1:500 in 2.5% NGS) to visualize osteogenic formation and anti-CD31 primary antibody (1:500 in 2.5% NGS) to visualize endotheliogenic differentiation. After three DPBS washes,

Table 1. Spheroid Groups Transfected with miRs and the Control Groups

Stage	*Group name*	*Description*
Initial Stage	2Day-O + 2 Day-E	Spheroids formed by ADSCs after 2 days of transfection by miR-148b, and $CD34^+/CD31^-$ cells after 2 days of transfection by miR-210 cultured for 28 days in basal medium
	2 Day-O + 6 Day-E	Spheroids formed by ADSCs after 2 days of transfection by miR-148b, and $CD34^+/CD31^-$ cells after 6 days of transfection by miR-210 cultured for 28 days in basal medium
	2 Day-O + 12 Day-E	Spheroids formed by ADSCs after 2 days of transfection by miR-148b, and $CD34^+/CD31^-$ cells after 12 days of transfection by miR-210 cultured for 28 days in basal medium
Early Stage	6 Day-O + 2 Day-E	Spheroids formed by ADSCs after 6 days of transfection by miR-148b, and $CD34^+/CD31^-$ cells after 2 days of transfection by miR-210 cultured for 28 days in basal medium
	6 Day-O + 6Day-E	Spheroids formed by ADSCs after 6 days of transfection by miR-148b, and $CD34^+/CD31^-$ cells after 6 days of transfection by miR-210 cultured for 28 days in basal medium
	6 Day-O + 12 Day-E	Spheroids formed by ADSCs after 6 days of transfection by miR-148b, and $CD34^+/CD31^-$ cells after 12 days of transfection by miR-210 cultured for 28 days in basal medium
Middle Stage	12 Day-O + 2 Day-E	Spheroids formed by ADSCs after 12 days of transfection by miR-148b, and $CD34^+/CD31^-$ cells after 2 days of transfection by miR-210 cultured for 28 days in basal medium
	12 Day-O + 6 Day-E	Spheroids formed by ADSCs after 12 days of transfection by miR-148b, and $CD34^+/CD31^-$ cells after 6 days of transfection by miR-210 cultured for 28 days in basal medium
	12 Day-O + 12 Day-E	Spheroids formed by ADSCs after 12 days of transfection by miR-148b, and $CD34^+/CD31^-$ cells after 12 days of transfection by miR-210 cultured for 28 days in basal medium
Controls	Positive Control Group	Spheroids formed by $CD34^+/CD31^-$ cells and ADSCs cultured for 28 days in osteogenic induction medium
	Negative Control Group	Spheroids formed by $CD34^+/CD31^-$ cells and ADSCs cultured for 28 days in basal medium

the samples were incubated with goat antimouse Alexa Fluor 488 secondary antibody (1:200 in 2.5% NGS), goat antirabbit Alexa Fluor 647 secondary antibody (1:200 in 2.5% NGS), and 4′,6-diamidino-2-phenylindole (DAPI; 1:200 in 2.5% NGS) for 3 h. Stained samples were examined with a Zeiss LSM 880 Airyscan confocal microscope.

To confirm spheroid morphologies, sectioned samples were also stained with hematoxylin and eosin (H&E) using the Leica Autostainer XL based on the manufacturer's protocol. After the staining process, stained sections were mounted using a xylene substitute mountant (Thermo Scientific, Waltham, MA) and stored at room temperature for drying overnight. Stained samples were imaged using an EVOS (Invitrogen, Waltham, MA) Auto FL microscope.

Alizarin Red S Staining

Using the Leica Autostainer, sections were dewaxed and then stained with Alizarin Red S in accordance with standard protocols. In brief, slices were incubated for 2 h at room temperature with Alizarin Red solution (EMD Millipore Corp., Billerica, MA). After removing excess dye, four Deionized Water (DI water) washes were performed. Coverslips were mounted to slides using the Xylene Substitute Mountant after being allowed to dry for 20 min at

Table 2. Primer Sequences for Measured mRNAs by Reverse Transcriptase-Polymerase Chain Reaction

mRNA	*Forward primer (5′→3′)*	*Reverse primer (5′→3′)*
RUNX2	GGTTAATCTCCGCAGGTCACT	CACTGTGCTGAAGAGGCTGTT
COL1	ATGACTATGAGTATGGGGAAGCA	TGGGTCCCTCTGTTACACTTT
BMP4	TAGCAAGAGTGCCGTCATTCC	GCGCTCAGGATACTCAAGACC
OCN	TCACACTCCTCGCCCTATTG	TCGCTGCCCTCCTGCTTG
ALP	AGCTGAACAGGAACAACGTGA	CTTCATGGTGCCCGTGGTC
BSP	AACGAAGAAAGCGAAGCAGAA	TCTGCCTCTGTGCTGTTGGT
PECAM-1	TAATACAACATCCACGAGGGTCC	ACAAAATTGCTTGCTAAAGAAGTGG
ANGPT-1	GTTCAGTCAGGGGAGCAGAG	CTCCAGACCCACCACAAGAT
GAPDH	ATGGGGAAGGTGAAGGTCG	GGGGTCATTGATGGCAACAATA

room temperature. The EVOS Auto FL microscope was used to image differentiated cells with mineral deposits by staining them brilliant red.

Statistical analysis

Each value was presented as mean ± standard deviation. One-way analysis of variance (ANOVA) was used to examine multiple comparisons, and a *post hoc* Tukey's multiple-comparison test was used to identify the individual differences through groups. At $*p < 0.05$, $**p < 0.01$, $***p < 0.001$, and $****p < 0.0001$, differences were deemed significant. GraphPad Software Inc., La Jolla, California's Prism software was used for all statistical analysis.

Results

Initial Stage Differentiation of Heterotypic Cellular Spheroids

To investigate the impact on codifferentiation of heterotypic cellular spheroids, as a function of miRNA mimic treatment group and induction time, on the formation of mineralized bone-like tissue with osteogenic and endothelial induction, we examined three different differentiation stages denoted as initial, early, and middle, assigned based on the osteogenic induction time (Table 1). Differentiation potential of these groups was characterized in detail and an effective differentiation timeline was established before combining inducted cells into spheroids to enable the formation of a prevascularized bone model (Fig. 1).

For the initial stage group, spheroids were formed using 2-day miR-148b (osteogenic) transfected ADSCs and miR-210 (endothelial) transfected $CD34^+/CD31^-$ cells at 2-, 6-, or 12 days after transfection. These cells were combined at a 4:1 ratio of ADSCs to $CD34^+/CD31^-$ cells and cultured for 28 days in total in basal medium. In the early-stage group, spheroids were formed using 6-day miR-148b transfected ADSCs and miR-210 transfected $CD34^+/CD31^-$ cells at 2-, 6-, and 12 days after transfection at the same 4:1 ratio and again cultured for 28 days in basal medium. For the middle stage group, spheroids were formed using 12-day miR-148b-transfected ADSCs and miR-210-transfected $CD34^+/CD31^-$ cells at 2-, 6-, and 12 days after transfection at the same 4:1 ratio and cultured for 28 days in basal medium (Fig. 1). In the positive control group, spheroids were prepared using nontransfected ADSCs and nontransfected $CD34^+/CD31^-$ cells mixed at a 4:1 ratio and cultured for 28 days in total in osteogenic induction medium. In the negative control group, spheroids were prepared using nontransfected ADSCs and nontransfected $CD34^+/CD31^-$ cells mixed at a 4:1 ratio and cultured for 28 days in basal medium. All of the experimental groups are defined and presented in Table 1. On days 14 and 28, spheroids were collected for analysis of all groups.

For all stages and groups, osteogenic and endothelial differentiation of heterotypic spheroids were validated using immunofluorescence (IF) staining showing RUNX2 and PECAM-1 counterstained with DAPI, respectively.

Confocal images of the initial stage group showed the strongest expression of RUNX2 when 2-day miR-148b-transfected ADSCs and 12-day miR-210-transfected $CD34^+/CD31^-$ cells were combined (2 Day-O + 12 Day-E) and cultured for 4 weeks (Fig. 2a). Although all initial stage groups showed similar level of RUNX2 expression at week 1, the group with 12-day $CD34^+/CD31^-$ cell transfection developed more evident RUNX2 expression at week 4 (Fig. 2a). Whereas IF images demonstrated that PECAM-1 staining expressed well for all initial-stage groups at

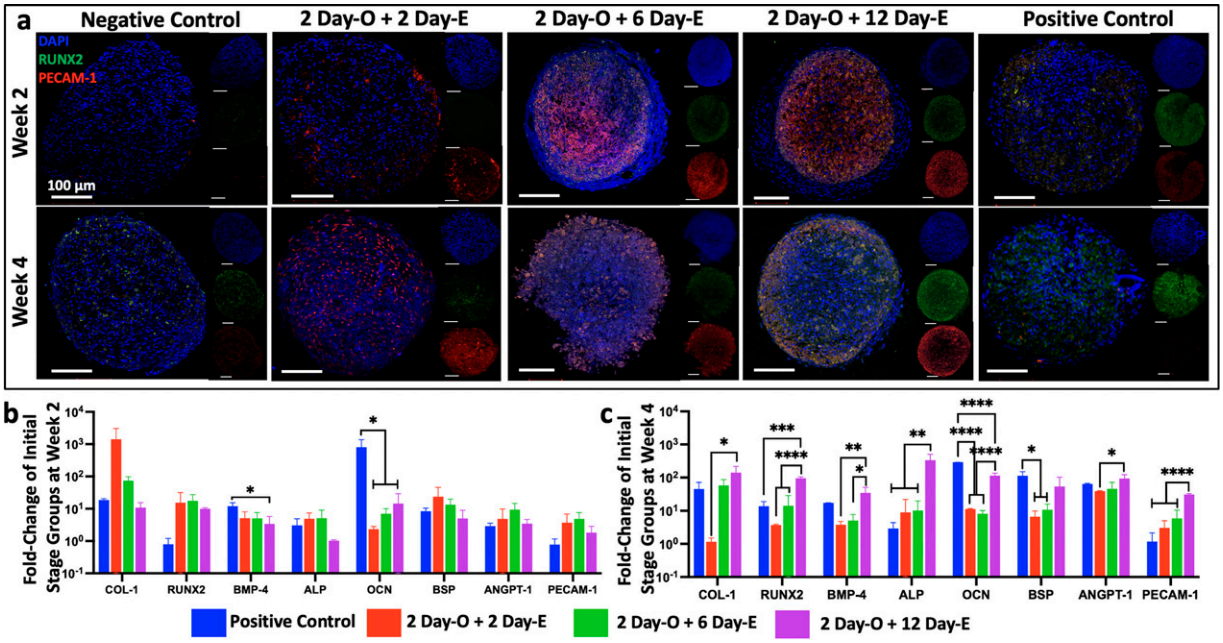

FIG. 2. **(a)** Immunostaining (DAPI in *blue*, RUNX2 in *green*, and PECAM-1 in *red*) images of initial-stage groups at weeks 2 and 4. Gene expression levels of initial-stage groups for osteogenic and endothelial markers at **(b)** weeks 2 and **(c)** 4. Scale bars in insets correspond to 100 µm ($n = 3$; $p* < 0.05$; $p** < 0.01$; $p*** < 0.001$; $p**** < 0.0001$). DAPI, 4′,6-diamidino-2-phenylindole; RUNX, runt-related transcription factor-2; PECAM-1, platelet/endothelial cell adhesion molecule-1.

weeks 2 and 4 (Fig. 2a). IF results for the initial-stage groups showed that 2 days of miR-148b mimic transfection in ADSCs did not induce robust osteogenic differentiation until they were combined with 12 days miR-210-transfected $CD34^{+}/CD31^{-}$ cells in the same spheroid environment for 4 weeks (Fig. 2a).

The relative expression of osteogenic gene markers, including COL-1, RUNX2, BMP-4, ALP, OCN, and BSP, and endotheliogenic gene markers, including PECAM-1 and ANGPT-1, were assessed using RT-PCR for the initial stage groups at weeks 2 and 4 (Figs. 2b, c). There was no significant difference among transfected initial stage groups at week 2. However, spheroids cultured in osteogenic induction medium (positive control) showed significantly higher gene expression than transfected groups for BMP-4 and OCN markers at week 2 (Fig. 2b). Similar to IF image results, RUNX2 gene expression was ~26-, 7-, and 7-fold higher in 2 Day-O + 12 Day-E group compared with the groups including 2 Day-O + 2 Day-E, 2 Day-O + 6 Day-E, and the positive control, respectively, at week 4 (Fig. 2c). Overall, all osteogenic markers but BSP showed significantly higher gene expression in 2 Day-O + 12 Day-E group as compared with other transfected groups at week 4. For the endothelial genes ANGPT-1 and PECAM-1, there were no significant difference between groups at week 2. Although PECAM-1 was ~10-, 5.3-, and 26.5-fold higher in 2 Day-O + 12 Day-E group compared with 2 Day-O + 6 Day-E, and positive control groups, respectively at week 4. For the initial stage groups, both IF and RT-PCR results indicate that 12-day miR-210 mimic transfection supported higher level of osteogenic differentiation in spheroids, whereas 2 days miR-210 transfection was capable for endotheliogenic differentiation with a combination of 2 days of miR-148b transfection at week 4.

To demonstrate the mineralization potential of spheroids for all groups, Osteoimage™ staining, an indicator staining for hydroxyapatite deposition during bone formation, was performed at weeks 2 and 4. The 2 Day-O + 12 Day-E group exhibited the strongest fluorescent intensity among the initial stage groups at week 4 (Fig. 3). However, all transfected groups showed a large cluster of mineralization similar to the positive control for the initial stage at week 4 (Fig. 3).

H&E images of spheroids of the initial stage group demonstrated no significant difference between transfected groups at week 2 (Fig. 4). Spheroids of the 2 Day-O + 12 Day-E group showed stronger bone matrix deposition as compared with other groups at week 4 (Fig. 4). In order to further confirm the morphology and osteogenic differentiation of the initial stage group spheroids, Alizarin Red staining was also performed at weeks 2 and 4. Spheroids of the 2 Day-O + 12 Day-E group exhibited the strongest Alizarin Red staining among the initial stage groups similar to the positive control during the 4-week differentiation process (Fig. 4).

Early-Stage Differentiation of Heterotypic Cellular Spheroids

Confocal images of the early-stage group showed that spheroids formed by 6-day miR-148b-transfected ADSCs with either 6-day or 12-day miR-210-transfected $CD34^{+}/CD31^{-}$ cells exhibited a similar staining trend for RUNX2 with the positive control group at week 2. However, the 6 Day-O + 12 Day-E group showed greater staining of RUNX2, whereas the 6 Day-O + 6 Day-E group showed similar expression of RUNX2 as compared with weeks 2 and 4. Moreover, IF images of PECAM-1 exhibited a

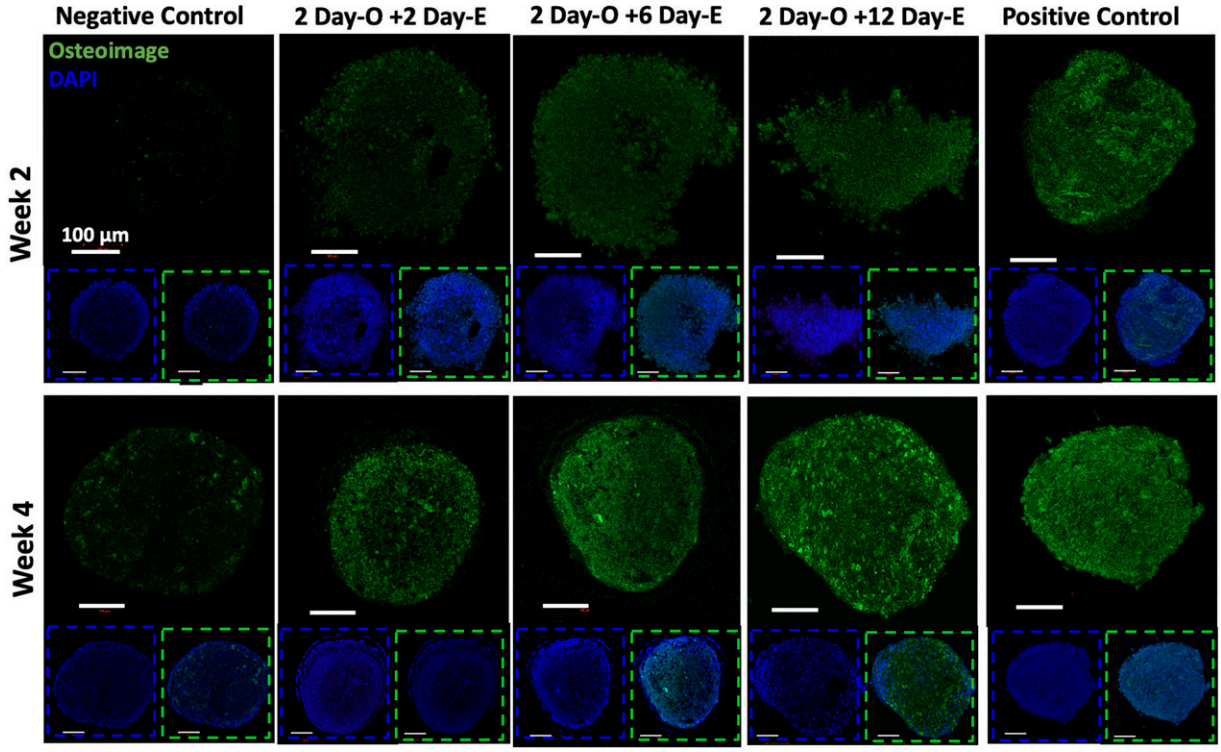

FIG. 3. Osteoimage™ staining of the initial-stage group spheroids along with negative and positive controls at weeks 2 and 4.

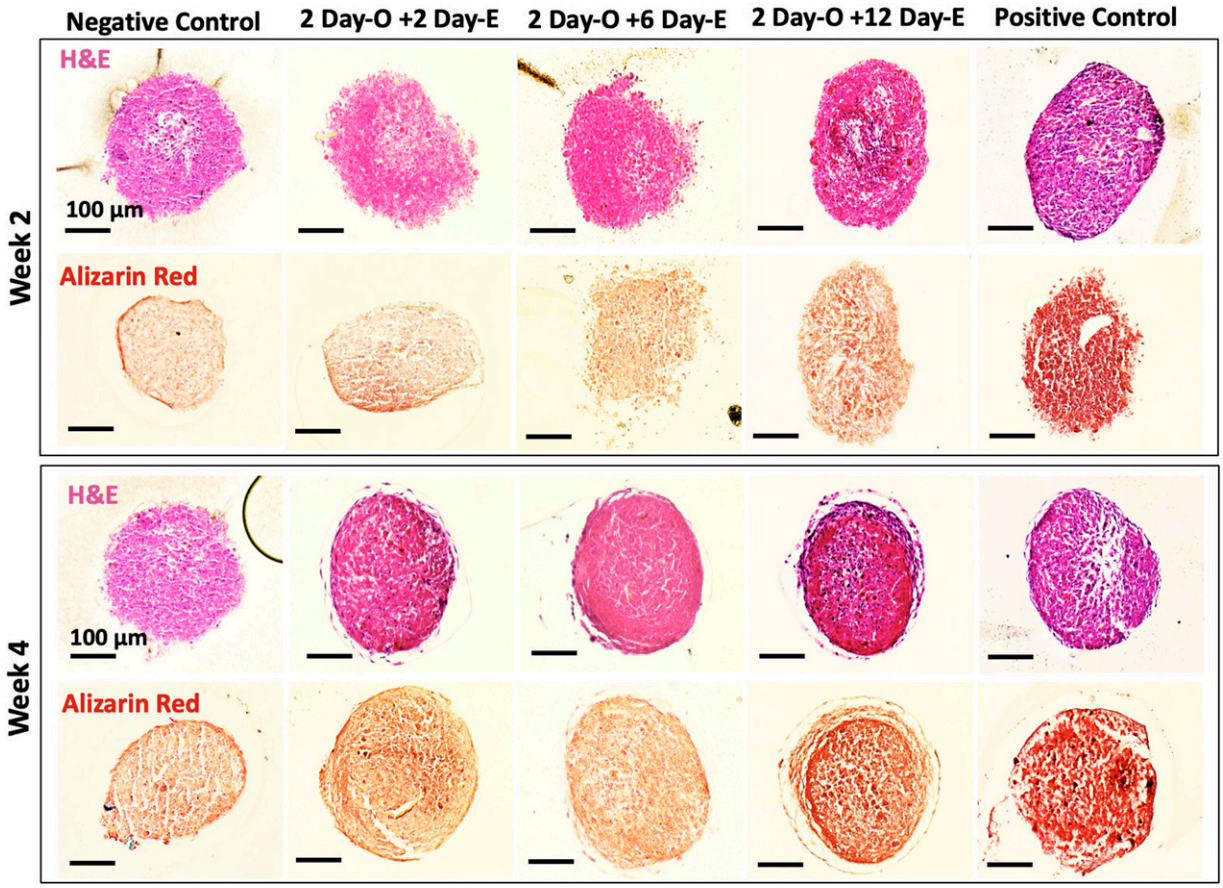

FIG. 4. Alizarin Red and H&E staining for the initial-stage group spheroids along with negative and positive controls at weeks 2 and 4. H&E, hematoxylin and eosin.

stronger expression for spheroids of the 6 Day-O + 2 Day-E or the 6 Day-O + 6 Day-E groups at week 4. Interestingly, the 6 Day-O + 12 Day-E group exhibited the strongest RUNX2 expression, whereas the 6 Day-O + 2 Day-E group exhibited the strongest PECAM-1 expression at week 4 (Fig. 5a).

Gene expression of osteogenic and endotheliogenic markers was also quantified by qRT-PCR for the early-stage groups at weeks 2 (Fig. 5b) and 4 (Fig. 5c). The OCN marker showed significantly higher gene expression for the positive control group as compared with other transfected groups at week 2 (Fig. 5b). There were no significant differences among the early-stage groups pertaining to RUNX2, ALP, BSP, and ANGPT-1 gene markers at week 2 (Fig. 5b). In general, there was an increased expression of these markers for the 6 Day-O + 12 Day-E group at week 4 compared with those at week 2. The 6 Day-O + 12 Day-E group had a significant difference for the expression of PECAM-1 as compared with other groups at weeks 2 and 4. Overall, RT-PCR for the early-stage group results indicated that 12-day miR-210 mimic transfection supported a higher level of osteogenic and endotheliogenic differentiation in spheroids at week 4 (Fig. 5c).

For the early-stage group spheroids, there were no significant difference among groups in terms of Osteoimage™ staining at week 2. However, the 6 Day-O + 6 Day-E group showed decreased calcium deposition at week 4 as compared with that at week 2. Overall, all groups but the 6 Day-O + 6 Day-E group exhibited large clusters of calcium deposition as similar to the positive control group at weeks 2 and 4 (Fig. 6).

Alizarin Red staining of the early-stage group spheroids exhibited a substantial staining for calcium deposition on both the 6 Day-O + 2 Day-E and 6 Day-O + 12 Day-E groups at week 4. Although spheroids of the 6 Day-O + 6 Day-E group demonstrated less Alizarin Red staining as compared with other transfected groups, the same group demonstrated a high-density Extra Cellular Matrix (ECM) deposition, which was visualized with a dark pink color at week 4 (Fig. 7). H&E images for the 6 Day-O + 2 Day-E and the 6 Day-O + 6 Day-E groups showed mostly nonmineralized tissue formation, which was identified as light pink color at week 2, but increasing the transfection time of miR-210 transfection (6 Day-O + 6 Day-E) resulted in improved matrix deposition at week 4 (Fig. 7).

Middle-Stage Differentiation of Heterotypic Cellular Spheroids

For the middle-stage group spheroids, there was no significant difference between groups at Week 2 based on confocal images (Fig. 8). Confocal images of middle-stage showed that spheroids formed by 12-day miR-148b mimic-transfected ADSCs with either 6-day or 12-day miR-210 mimic-transfected $CD34^+$/$CD31^-$ cells exhibited similar trend for RUNX2 expression with respect to the positive control group at week 2. The 12 Day-O + 12 Day-E group showed a decreased RUNX2 staining at week

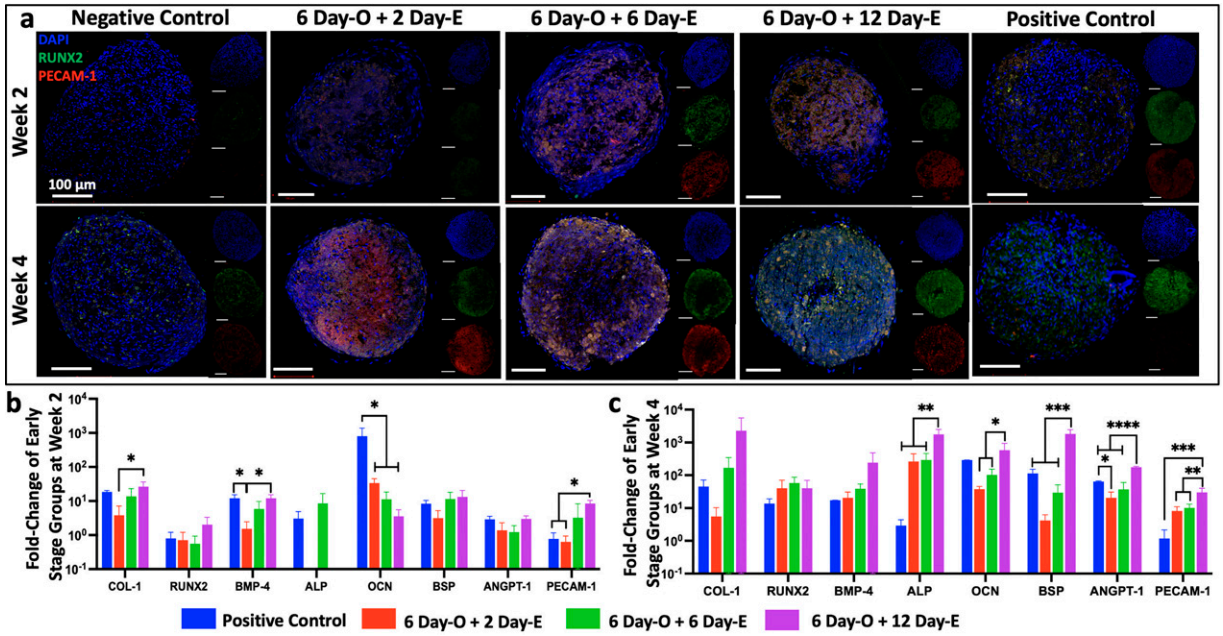

FIG. 5. **(a)** Immunostaining (DAPI in *blue*, RUNX2 in *green*, and PECAM-1 in *red*) images of early-stage groups at weeks 2 and 4. Gene expression levels of early-stage groups for osteogenic and endothelial markers at **(b)** weeks 2 and **(c)** 4. Scale bars in insets correspond to 100 µm ($n = 3$; $p^* < 0.05$; $p^{**} < 0.01$; $p^{***} < 0.001$; $p^{****} < 0.0001$).

4 as compared with week 2. Moreover, IF images stained for PECAM-1 exhibited a strong of the expression for spheroids of the 12 Day-O + 2 Day-E or 12 Day-O + 6 Day-E groups at week 4. Interestingly, the 12 Day-O + 12 Day-E group exhibited the strongest RUNX2 expression, whereas the 12 Day-O + 2 Day-E group exhibited the strongest PECAM-1 expression at week 4 (Fig. 8a).

As described before, RT-PCR was used to check gene expression level of osteogenic and endotheliogenic markers for the middle-stage groups at weeks 2 (Fig. 8b) and 4 (Fig. 8c). The results revealed significantly higher OCN expression for the positive control group as compared with other transfected groups similar to results with initial and early-stage groups at week 2 (Fig. 8b). There were no significant

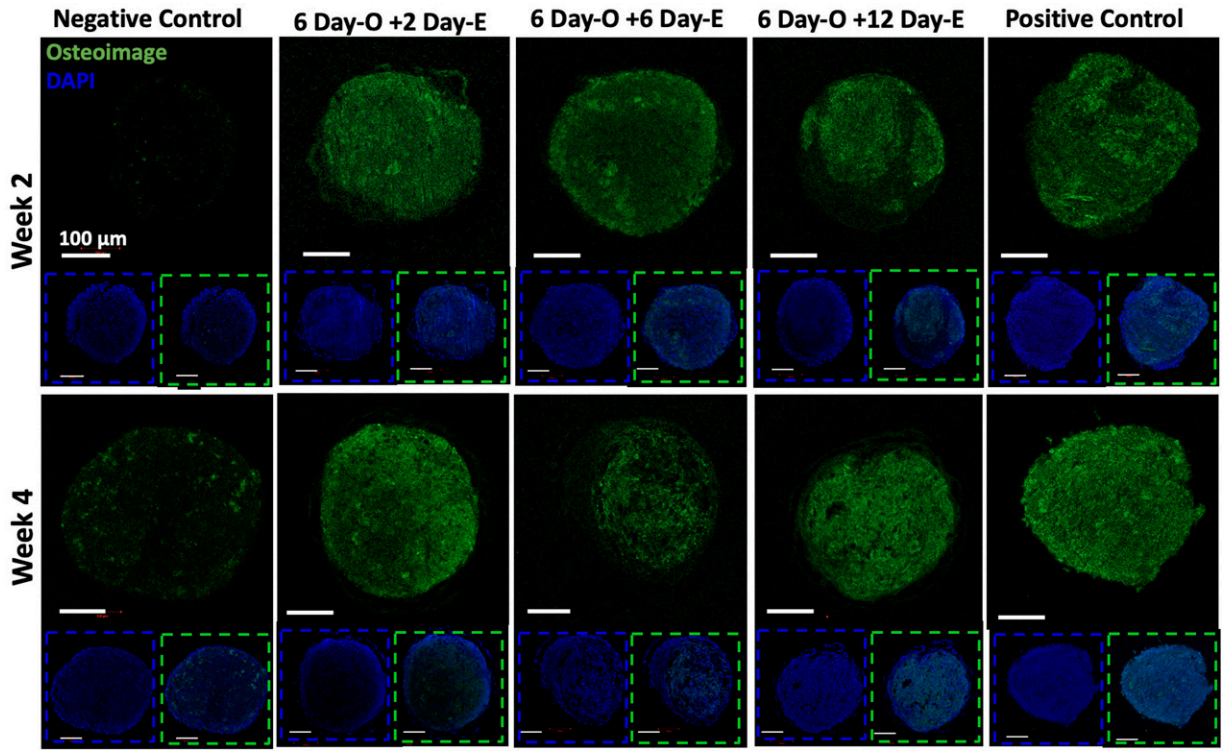

FIG. 6. Osteoimage™ staining of the early-stage group spheroids along with negative and positive controls at weeks 2 and 4.

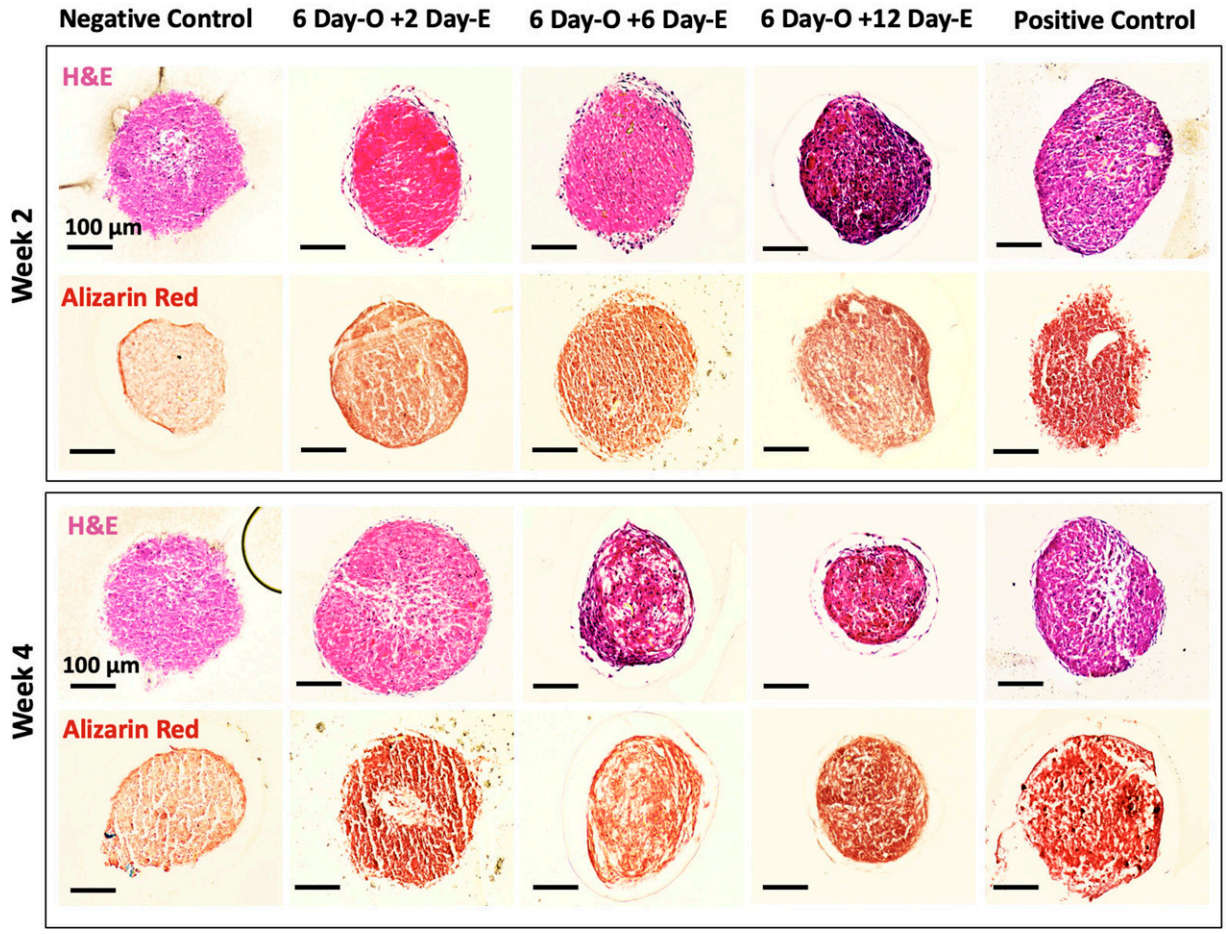

FIG. 7. Alizarin Red and H&E staining for the early-stage group spheroids along with negative and positive controls at weeks 2 and 4.

differences among the early-stage groups in the expression of RUNX2, ALP, BSP, and COL-1 at week 2 (Fig. 8a). There was increased expression of all genes in the 12 Day-O + 2 Day-E group at week 4 compared with those at week 2. Overall, RT-PCR results indicate that 12-day of miR-148b transfection supported higher level of osteogenic and endotheliogenic differentiation in spheroids when cocultured with 2-day miR-210 transfected $CD34^{+}/CD31^{-}$ progenitors at week 4 (Figs. 8b–c).

For the middle-stage group spheroids, there were no significant difference among groups except the negative control group in terms of Osteoimage™ staining at week 2. The 12 Day-O + 2 Day-E and the 12 Day-O + 6 Day-E groups showed increased calcium deposition at week 4 as compared with those at week 2. Overall, all groups showed considerable amount of calcium deposition at weeks 2 and 4 (Fig. 9).

Alizarin Red staining of the middle-stage group spheroids exhibited a large red staining cluster as showing calcium deposition for both the 12 Day-O + 2 Day-E and the 12 Day-O + 6 Day-E groups at week 4. Although, spheroids of the 12 Day-O + 12 Day-E group demonstrated less Alizarin Red staining as compared with other groups, the same group demonstrated a high-density ECM deposition, which was visualized with a dark pink color in the H&E images at week 4 (Fig. 10).

Discussion

In the recent years, we have substantially advanced our understanding of the molecular contributors to osteogenic and endotheliogenic commitment and maturation. However, coculturing of progenitor cells in *in vitro* tissue models result in complex interactions, which lead to difficulties in predicting the differentiation outcomes. Understanding how the heterotypic progenitors interact with each other in these models serves as a useful tool to study the phenomena of codifferentiation and progenitor cell crosstalk. In this study, we demonstrated an alternative differentiation strategy where miR-148b- and -210 mimic-transfected progenitor cells were combined into heterotypic cellular spheroids to be able to understand how progenitor maturity impacts heterotypic differentiation as a model for vascularized bone formation.

This system, using miR mimics to *de novo* induce differentiation, was found to be more straightforward to implement compared with the use of a mixture of osteogenic and endotheliogenic medium for heterotypic cell culture, which can result in competitive differentiation signals, and hence failures of differentiation. A coculture's potential of success depends on a wide range of variables, causing it to be a complicated and unpredictable system.[45] For example, cellular secretions consist of extracellular vesicles and molecules which have both local and distal effects referred to as paracrine signaling.[46]

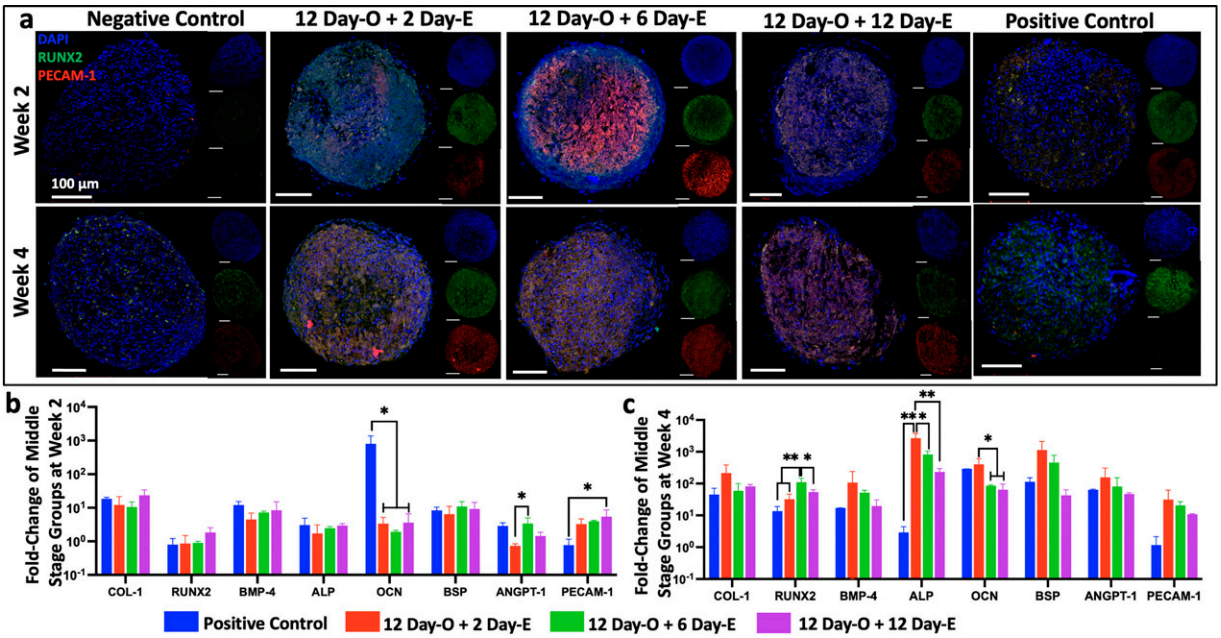

FIG. 8. **(a)** Immunostaining (DAPI in *blue*, RUNX2 in *green*, and PECAM-1 in *red*) images of middle-stage groups at weeks 2 and 4. Gene expression levels of middle-stage groups for osteogenic and endothelial markers at **(b)** weeks 2 and **(c)** 4. Scale bars in insets correspond to 100 µm ($n = 3$; $p^* < 0.05$; $p^{**} < 0.01$; $p^{***} < 0.001$; $p^{****} < 0.0001$).

Paracrine signaling is a way of cell-to-cell or cell-to-tissue communication, where a cell releases out a signal that modifies the function or differentiation of neighboring cells or tissue.[47] Paracrine factors can induce surrounding cells to differentiate into mature cells and modulate the activity of stem and progenitor cells that secrete paracrine signals.[48] Cells from different lineages and from the same cell lineages can communicate with each other via paracrine signaling.[47] In our study, we evaluated the effect of paracrine signaling on the codifferentiation of ADSCs and $CD34^+/CD31^-$ cells toward osteogenic and endotheliogenic lineages driven by miR-148b and -210 mimics, respectively. In particular, we examined the differentiation markers as a function of maturation time after transfection. We realized that while miR-210 mimic induced the endotheliogenic

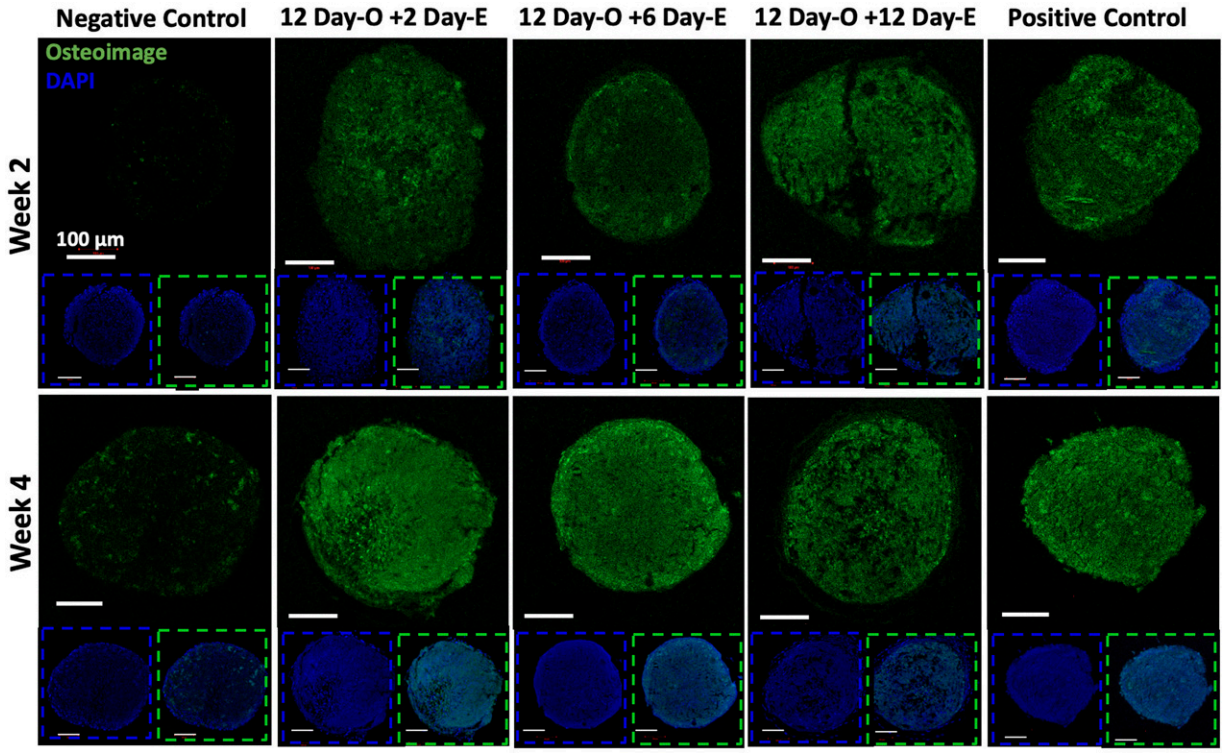

FIG. 9. Osteoimage™ staining of the middle-stage group spheroids along with negative and positive controls at weeks 2 and 4.

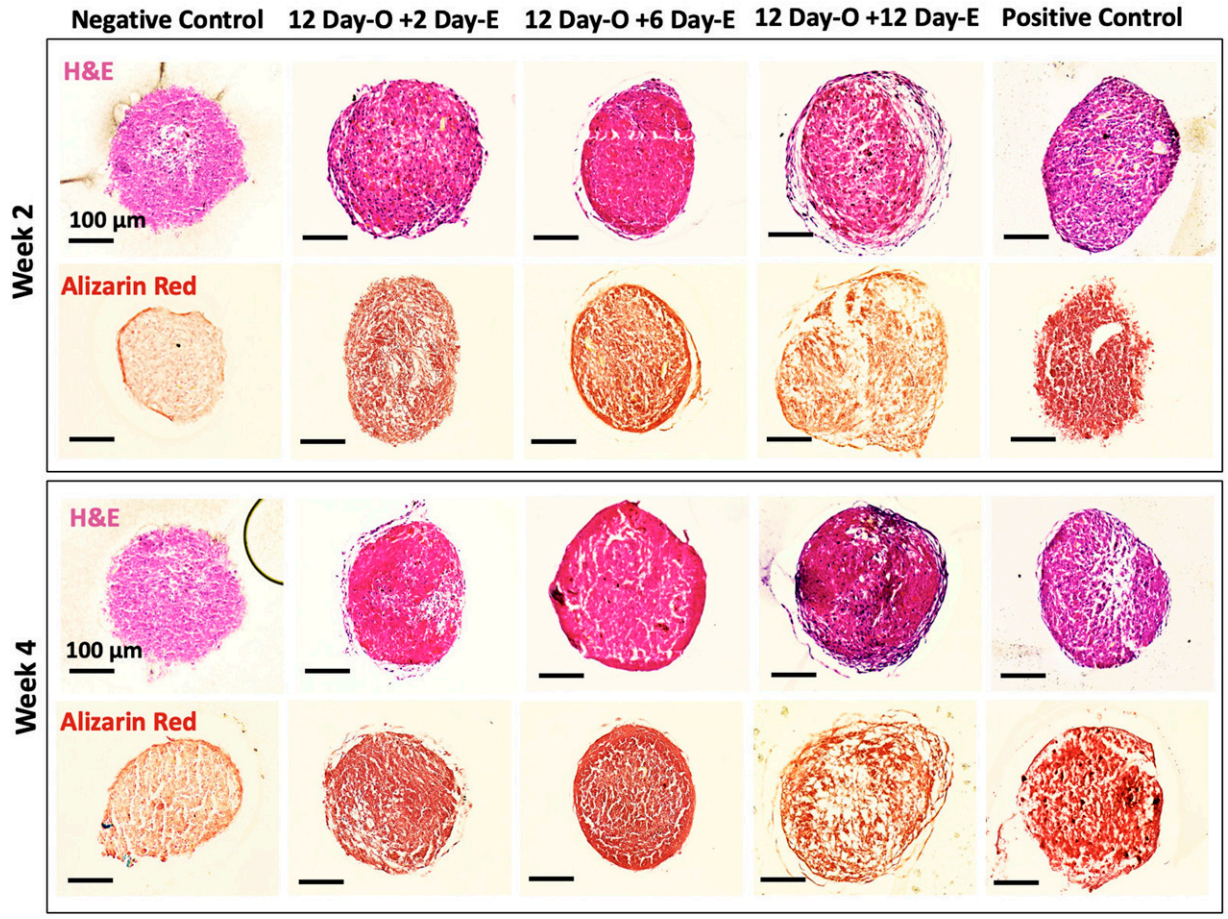

FIG. 10. Alizarin Red and H&E staining for the middle-stage group spheroids along with negative and positive controls at weeks 2 and 4.

differentiation of $CD34^+/CD31^-$ cells after only 2 days of transfection in 2D culture (Fig. 2), miR-148b mimic required a minimum of 6 days of 2D culture to stably induce the osteogenic differentiation of ADSCs (Figs. 5–6).

Blood vessel formation *in situ* by vascular stem/progenitor cells is known as vasculogenesis.[49,50] It has recently been reported that EPCs influence postnatal vasculogenesis processes.[50] However, the process for developing stable blood vessels is complicated and necessitates coordinated interactions between ECs, and cells and tissues of the surrounding environment such as osteoprogenitors of regenerating bone tissue.[51] On the other hand, during the development of long bones, VEGF expression is upregulated before the formation of blood vessels and is associated with the osteogenesis process.[52] Indeed, it has been shown that the hypoxia inducible factor-α (HIF-α) pathway plays a crucial role in coordinating osteogenesis and vascularization during the creation of long bones[53] and miR-210 mimic over expression is known to induce increased HIF-α.[37,54] This increase in bone formation is owing to enhanced vasculogenesis activity, which is mediated by elevated levels of VEGF in HIF-α overexpressing osteoblasts.[55]

Multiple studies have shown that that the ability of stem cells to secrete soluble factors, such as paracrine signals that alter the tissue microenvironment, could have a greater impact than their cellular transdifferentiation in affecting tissue formation.[56,57] Our results showed that 2 days after miR-210 transfection of $CD34^+/CD31^-$ cells were sufficient to induce endotheliogenic differentiation, regardless of the duration (2-, 6-, or 12-day) of miR-148b mimic induction of ADSCs before forming spheroids. However, miR-148b-transfected ADSCs were affected by the maturity of miR-210-transfected $CD34^+/CD31^-$ cells. Longer posttransfection culture of miR-210-induced $CD34^+/CD31^-$ cells had a greater influence on the fate and differentiation of miR-148b transfected ADSCs into a heterotypic spheroid form, resulting in better osteogenic properties.

The interplay between miR-148b and −210 transfection also resulted in antagonistic cross-talk between miR-induced progenitors if the posttransfection time was same, i.e., both ADSCs and $CD34^+/CD31^-$ cultured for 2, 6, or 12 days before spheroid formation. This indicated that progenitors might have a negative impact during the differentiation of surrounding immature cells depending on the maturity of the progenitor population.

Conclusion

In this study, we fabricated heterotypic cellular spheroids of ADSCs and $CD34^+/CD31^-$ cells after their transfection by miR-148b and -210, respectively. It was found that the maturity of differentiating progenitors could have a significant impact on the codifferentiation of heterotypic cultures. Both agonistic and antagonistic cross-talk was observed between miR-induced progenitors depending on the relative maturity of these osteogenic and endotheliogenic progenitors. When

osteogenic and endotheliogenic progenitors of similar maturity were combined in a spheroid, both osteogenic and endotheliogenic marker expression was reduced, compared with the spheroids made of progenitors with dissimilar maturity.

Acknowledgments

The reagents were provided by R&D Systems (Minneapolis, MN), for which the authors are thankful.

Data Availability

This article contains all the information required to assess the results obtained via this work. You may ask the authors for additional data regarding this article.

Author Disclosure Statement

I.T.O. is a member of the scientific advisory boards for Healshape and Biolife4D, he has an equity stake in Biolife4D. Other authors declare that there are no known conflicts of interest pertaining to this article, and there has not been any substantial funding for the study that would have had an impact on its outcomes.

Funding Information

The National Science Foundation provided funding for this work under grant numbers 1914885 (I.T.O.), and 2033673 (D.J.H.), and the National Institute Health provided funding under award numbers R01DE028614 (I.T.O.), R01EB034566 (I.T.O.), and RDE024790A (D.J.H.). The National Institutes of Health and the National Science Foundation may not have approved the author's views, interpretations, conclusions, or recommendations.

Supplementary Material

Supplementary Figure S1
Supplementary Figure S2
Supplementary Figure S3

References

1. Alonzo M, Primo FA, Kumar SA, et al. Bone tissue engineering techniques, advances, and scaffolds for treatment of bone defects. Curr Opin Biomed Eng 2021;17(100248)
2. Chai M, Gu C, Shen Q, et al. Hypoxia alleviates dexamethasone-induced inhibition of angiogenesis in co cultures of HUVECs and rBMSCs via HIF-1α. Stem Cell Res Ther 2020;11(1):1–13.
3. Mercado-Pagán ÁE, Stahl AM, Shanjani Y, et al. Vascularization in bone tissue engineering constructs. Ann Biomed Eng 2015;43(3):718–729.
4. McKee C, Chaudhry GR. Advances and challenges in stem cell culture. Colloids and Surfaces B: Biointerfaces 2017; 159:62–77.
5. Saran U, Piperni SG, Chatterjee S. Role of angiogenesis in bone repair. Arch Biochem Biophys 2014;561:109–117.
6. Asserson DB, Orbay H, Sahar DE. Review of the pathways involved in the osteogenic differentiation of adipose-derived stem cells. Journal of Craniofacial Surgery 2019;30(3):703–708.
7. Rautiainen S, Laaksonen T, Koivuniemi R. Angiogenic effects and crosstalk of adipose-derived mesenchymal stem/stromal cells and their extracellular vesicles with endothelial cells. Int J Mol Sci 2021;22(19):10890.
8. Kanczler J, Oreffo R. Osteogenesis and angiogenesis: The potential for engineering bone. Eur Cell Mater 2008;15(2): 100–114.
9. Souza LE, Beckenkamp LR, Sobral LM, et al. Pre-culture in endothelial growth medium enhances the angiogenic properties of adipose-derived stem/stromal cells. Angiogenesis 2018;21(1):15–22.
10. Sidney LE, Branch MJ, Dunphy SE, et al. Concise review: Evidence for CD34 as a common marker for diverse progenitors. Stem Cells 2014;32(6):1380–1389.
11. Liu L, Shi G-P. CD31: Beyond a marker for endothelial cells. Cardiovasc Res 2012;94(1):3–5.
12. Forghani A, Koduru SV, Chen C, et al. Differentiation of adipose tissue–derived CD34+/CD31− cells into endothelial cells *in vitro*. Regen Eng Transl Med 2020;6(1):101–110.
13. Liang T, Zhu L, Gao W, et al. Coculture of endothelial progenitor cells and mesenchymal stem cells enhanced their proliferation and angiogenesis through PDGF and Notch signaling. FEBS Open Bio 2017;7(11):1722–1736.
14. Kocherova I, Bryja A, Mozdziak P, et al. Human umbilical vein endothelial cells (HUVECs) co-culture with osteogenic cells: From molecular communication to engineering prevascularised bone grafts. J Clin Med 2019;8(10):1602.
15. Merfeld-Clauss S, Lupov IP, Lu H, et al. Adipose stromal cell contact with endothelial cells results in loss of complementary vasculogenic activity mediated by induction of Activin A. Stem Cells 2015;33(10):3039–3051.
16. Verseijden F, Posthumus-van Sluijs SJ, Pavljasevic P, et al. Adult human bone marrow–and adipose tissue–derived stromal cells support the formation of prevascular-like structures from endothelial cells *in vitro*. Tissue Engineering Part A 2010;16(1):101–114.
17. Klar AS, Güven S, Zimoch J, et al. Characterization of vasculogenic potential of human adipose-derived endothelial cells in a three-dimensional vascularized skin substitute. Pediatr Surg Int 2016;32(1):17–27.
18. Periasamy R, Elshaer SL, Gangaraju R. CD140b (PDGFRβ) signaling in adipose-derived stem cells mediates angiogenic behavior of retinal endothelial cells. Regen Eng Transl Med 2019;5(1):1–9.
19. Rao RR, Stegemann JP. Cell-based approaches to the engineering of vascularized bone tissue. Cytotherapy 2013;15(11): 1309–1322.
20. Mutschall H, Winkler S, Weisbach V, et al. Bone tissue engineering using adipose-derived stem cells and endothelial cells: Effects of the cell ratio. J Cell Mol Med 2020; 24(12):7034–7043.
21. De Moor L, Merovci I, Baetens S, et al. High-throughput fabrication of vascularized spheroids for bioprinting. Biofabrication 2018;10(3).
22. Kuhn LT, Liu Y, Boyd NL, et al. Developmental-like bone regeneration by human embryonic stem cell-derived mesenchymal cells. Tissue Engineering Part A 2014;20(1-2):365–377.
23. Eppler SM, Combs DL, Henry TD, et al. A target-mediated model to describe the pharmacokinetics and hemodynamic effects of recombinant human vascular endothelial growth factor in humans. Clin Pharma and Therapeutics 2002;72(1):20–32.
24. Celik N, Kim MH, Hayes DJ, et al. miRNA induced co-differentiation and cross-talk of adipose tissue-derived progenitor cells for 3D heterotypic pre-vascularized bone formation. Biofabrication 2021;13(4).
25. Shi H, Zhao Z, Jiang W, et al. A review into the insights of the role of endothelial progenitor cells on bone biology. Front Cell Dev Biol 2022;10:878697.

26. Fakhry M, Hamade E, Badran B, et al. Molecular mechanisms of mesenchymal stem cell differentiation towards osteoblasts. World J Stem Cells 2013;5(4):136–148.
27. Kim EY, Moudgil KD. Regulation of autoimmune inflammation by pro-inflammatory cytokines. Immunol Lett 2008; 120(1-2):1–5.
28. Dong S, Yang B, Guo H, et al. MicroRNAs regulate osteogenesis and chondrogenesis. Biochem Biophys Res Commun 2012;418(4):587–591.
29. Lindsay MA. microRNAs and the immune response. Trends Immunol 2008;29(7):343–351.
30. Liao Y-H, Chang Y-H, Sung L-Y, et al. Osteogenic differentiation of adipose-derived stem cells and calvarial defect repair using baculovirus-mediated co-expression of BMP-2 and miR-148b. Biomaterials 2014;35(18):4901–4910.
31. Abu-Laban M, Hamal P, Arrizabalaga JH, et al. Combinatorial delivery of miRNA-nanoparticle conjugates in human adipose stem cells for amplified osteogenesis. Small 2019; 15(50):e1902864.
32. Qureshi AT, Doyle A, Chen C, et al. Photoactivated miR-148b–nanoparticle conjugates improve closure of critical size mouse calvarial defects. Acta Biomater 2015;12:166–173.
33. Li KC, Lo SC, Sung LY, et al. Improved calvarial bone repair by hASCs engineered with Cre/loxP-based baculovirus conferring prolonged BMP-2 and MiR-148b co-expression. J Tissue Eng Regen Med 2017;11(11):3068–3077.
34. Zaccagnini G, Greco S, Voellenkle C, et al. miR-210 hypoxamiR in Angiogenesis and Diabetes. Antioxidants & Redox Signaling 2022;36(10-12):685–706.
35. Zhuang Y, Cheng M, Li M, et al. Small extracellular vesicles derived from hypoxic mesenchymal stem cells promote vascularized bone regeneration through the miR-210-3p/EFNA3/PI3K pathway. Acta Biomater 2022;150:413–426.
36. Fasanaro P, D'Alessandra Y, Di Stefano V, et al. MicroRNA-210 modulates endothelial cell response to hypoxia and inhibits the receptor tyrosine kinase ligand Ephrin-A3. Journal of Biological Chemistry 2008;283(23):15878–15883.
37. Chan YC, Banerjee J, Choi SY, et al. miR-210: The master hypoxamir. Microcirculation 2012;19(3):215–223.
38. Guo L, Zhao RC, Wu Y. The role of microRNAs in self-renewal and differentiation of mesenchymal stem cells. Exp Hematol 2011;39(6):608–616.
39. Lian JB, Stein GS, Van Wijnen AJ, et al. MicroRNA control of bone formation and homeostasis. Nat Rev Endocrinol 2012;8(4):212–227.
40. Childs SG. Osteonecrosis: Death of bone cells. Orthopaedic Nursing 2005;24(4):295???301–301.
41. Lazzarini L, De Lalla F, Mader JT. Long bone osteomyelitis. Curr Infect Dis Rep 2002;4(5):439–445.
42. Burkhardt R, Kettner G, Böhm W, et al. Changes in trabecular bone, hematopoiesis and bone marrow vessels in aplastic anemia, primary osteoporosis, and old age: A comparative histomorphometric study. Bone 1987;8(3):157–164.
43. Celik N, Kim MH, Yeo M, et al. miRNA induced 3D bioprinted-heterotypic osteochondral interface. Biofabrication 2022;14(4).
44. Ayan B, Celik N, Zhang Z, et al. Aspiration-assisted freeform bioprinting of pre-fabricated tissue spheroids in a yield-stress gel. Commun Phys 2020;3(1):183.
45. Vis MA, Ito K, Hofmann S. Impact of culture medium on cellular interactions in *in vitro* co-culture systems. Front Bioeng Biotechnol 2020;8:911.
46. Madrigal M, Rao KS, Riordan NH. A review of therapeutic effects of mesenchymal stem cell secretions and induction of secretory modification by different culture methods. J Transl Med 2014;12(1):214–260.
47. Ferraris VA. How do cells talk to each other?: Paracrine factors secreted by mesenchymal stromal cells. J Thorac Cardiovasc Surg 2016;151(3):849–851.
48. Kusuma GD, Carthew J, Lim R, et al. Effect of the microenvironment on mesenchymal stem cell paracrine signaling: Opportunities to engineer the therapeutic effect. Stem Cells Dev 2017;26(9):617–631.
49. Johnson KE, Wilgus TA. Vascular endothelial growth factor and angiogenesis in the regulation of cutaneous wound repair. Adv Wound Care (New Rochelle) 2014;3(10):647–661.
50. Masuda H, Asahara T. Post-natal endothelial progenitor cells for neovascularization in tissue regeneration. Cardiovasc Res 2003;58(2):390–398.
51. Yin Y, Tang Q, Xie M, et al. Insights into the mechanism of vascular endothelial cells on bone biology. Biosci Rep 2021;41(1).
52. Duffy AM, Bouchier-Hayes DJ, Harmey JH. Vascular endothelial growth factor (VEGF) and its role in non-endothelial cells: Autocrine signalling by VEGF. In: Madame Curie Bioscience Database [Internet]. Landes Bioscience: Austin 2013.
53. Wang Y, Wan C, Deng L, et al. The hypoxia-inducible factor α pathway couples angiogenesis to osteogenesis during skeletal development. J Clin Invest 2007;117(6):1616–1626.
54. Liu P, Qin L, Liu C, et al. Exosomes derived from hypoxia-conditioned stem cells of human deciduous exfoliated teeth enhance angiogenesis via the transfer of let-7f-5p and mir-210-3p. Front Cell Dev Biol 2022;10:879877.
55. Hu K, Olsen BR. The roles of vascular endothelial growth factor in bone repair and regeneration. Bone 2016;91:30–38.
56. Phinney DG, Prockop DJ. Concise review: Mesenchymal stem/multipotent stromal cells: The state of transdifferentiation and modes of tissue repair—current views. Stem Cells 2007;25(11):2896–2902.
57. Prockop D. "Stemness" does not explain the repair of many tissues by mesenchymal stem/multipotent stromal cells (MSCs). Clin Pharmacol Ther 2007;82(3):241–243.

Address correspondence to:
Ibrahim T. Ozbolat
Engineering Science and Mechanics Department
The Pennsylvania State University
University Park
PA 16802
USA

E-mail: ito1@psu.edu

Daniel J. Hayes
Biomedical Engineering Department
The Pennsylvania State University
University Park
PA 16802
USA

E-mail: djh195@psu.edu

Received: September 29, 2023
Accepted: January 31, 2024
Online Publication Date: June 14, 2024